Society of Petroleum Engineers

SPE-184862-MS

New Age Fracture Mapping Diagnostic Tools-A STACK Case Study

K. Haustveit, K. Dahlgren, H. Greenwood, T. Peryam, and B. Kennedy, Devon Energy; M. Dawson, Statoil

This paper was prepared for presentation at the SPE Hydraulic Fracturing Technology Conference and Exhibition held in The Woodlands, Texas, USA, 24-26 January 2017.

Abstract

The application of learnings from an underground laboratory has led to significant completion changes in a world-class North American unconventional asset. Understanding the stimulated fracture geometry in unconventional reservoirs allows for optimal development of the asset. In this paper, we will review a case study comparing both new and commonly accepted technologies to quantify stimulated fracture geometry.

The technologies applied to improve the understanding of fracture geometry in this case study include fiber optic monitoring (Distributed Acoustic Sensing and Distributed Temperature Sensing), borehole microseismic, electromagnetic imaging, offset well pressure monitoring with IMAGE Frac technology, water hammer analysis, and fracture modeling. The validation tools used include a production interference test, Rate Transient Analysis (RTA), Oil Soluble Tracers (OST), and Fracture Fluid Identifiers (FFI).

Fiber optic monitoring was used to assess cluster efficiency, fluid and sand distribution per cluster and diverter effectiveness. Hydraulic half-lengths, heights, and fracture azimuth were estimated using a borehole microseismic system consisting of three vertical arrays and two horizontal arrays. Electromagnetic imaging provided insight on hydraulic half-length for 12 stages. Offset pressure monitoring provided hydraulic and propped half-lengths, heights, and fracture azimuth. The fracture model was calibrated using a diagnostic fracture injection test and vertical logs from the section of interest. Results from the technologies suggest an increase in well density is required to maximize the project net present value.

The offset well pressure data coupled with fiber optic monitoring led to optimization of diverter applications. A variety of completion variables were tested, including fluid design, proppant size, perforation designs and diverter types, results have been integrated into an improved completion design.

Introduction

A thorough understanding of fracture geometry and well spacing early in the development of a field can drastically improve the project net present value, this is especially true when developing stacked intervals. This paper will discuss a spacing pilot in the STACK (**S**ooner **T**rend **A**nadarko Basin **C**anadian and **K**ingfisher Counties). The STACK is located in the Anadarko Basin, the basin is home to several stacked intervals of reservoir. Figure 1 describes the five-well layout for this spacing pilot, Well C was equipped with fiber optic monitoring. The results from this work has led to an improvement in well spacing.

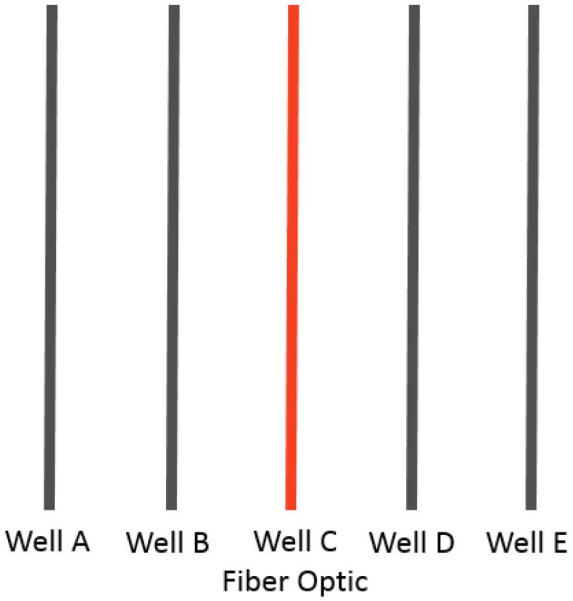

Figure 1— Well layout for spacing pilot

Diagnostic Tools

Several diagnostic tools were utilized to improve the understanding of fracture geometry. Each tool provided insight into different characteristics of the fracture geometry (hydraulic, propped, and conductive), integration of these results lead to optimization of the completion design.

Fiber Optic Monitoring

Distributed Acoustic Sensing (DAS) and Distributed Temperature Sensing (DTS) was used to analyze cluster efficiency and diversion effectiveness. DTS provides us with the ability to monitor both cool-down during hydraulic stimulation and warm-back before the well is produced (Ugueto et al. 2014). Diversion was identified through DAS and DTS evaluation. The results from DAS suggest strong heel bias was present in a majority of the stages. Interference between adjacent fractures within a given stage, and from adjacent fracture stages, results in a consistent geometric predominance for fracture growth in the most heel-ward perforation cluster (Wheaton et al. 2016). A variety of completions variables targeting improved fluid distribution were evaluated throughout the completion of the lateral. Notable variables include perforation designs, fluid systems, diverter, and proppant size. Two perforation designs were trialed on several stages resulting in improved fluid distribution when compared to the base perforation design. Results from DAS influenced a change to the timing of proppant size changes.

Figure 2 shows the proppant distribution of individual clusters for several stages of the fiber optic well (Well C). An algorithm applied to the DAS data provides the proppant volume placed into each cluster. The average proppant distribution in each stage shows a heelward bias.

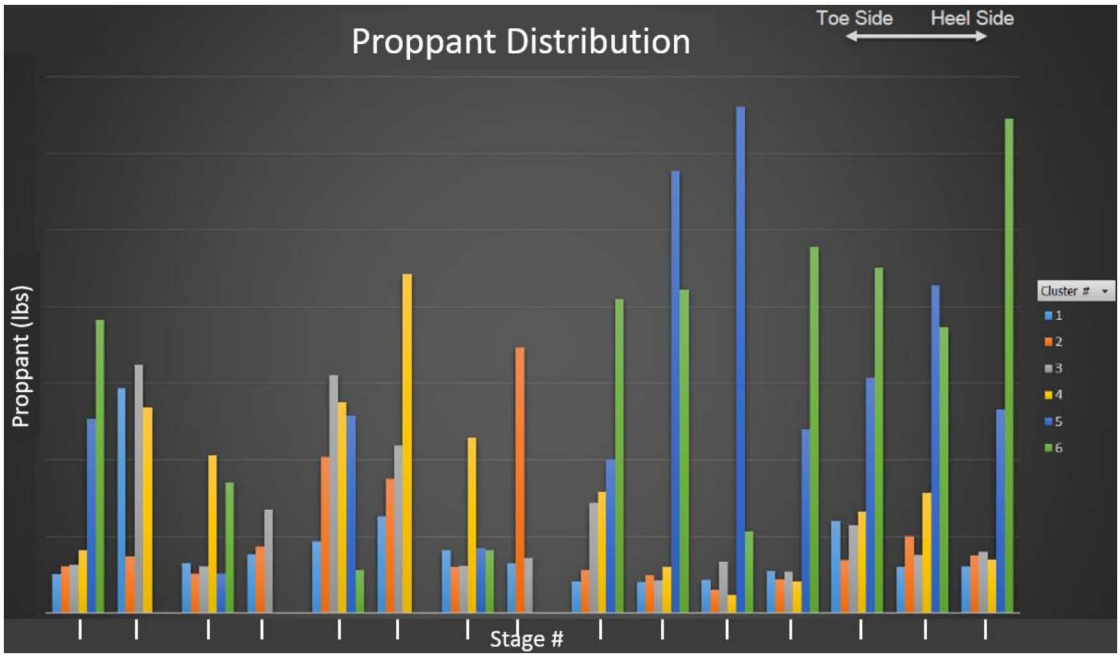

Figure 2— Proppant distribution per cluster from DAS

The ability to calculate the amount of fluid and proppant placed into each cluster aids in the calibration of fracture models resulting in improved forward modeling capabilities. Figures 3 and 4 show the results of the perforation design variable testing performed on the test well with two primary perforation design tested. With any alteration of the treatment schedule, both perforation designs were used in succession to normalize for these changes.

Figure 3 shows the proppant distributions of each stage as an absolute percent deviation from perfect efficiency and the distribution of all clusters. Each point on the plot represents a single cluster, zero percent deviation represents even distribution to each cluster, 100% deviation occurs when one-half of the clusters take two times the designed treatment. Perf design #2 averaged 18% improved distribution when compared to perf design #1. Based on modeling the improved distributions derived from fiber optic monitoring, perf design #2 creates more equal fracture heights and half-lengths, as well as increasing the overall number of effective fractures in the wellbore.

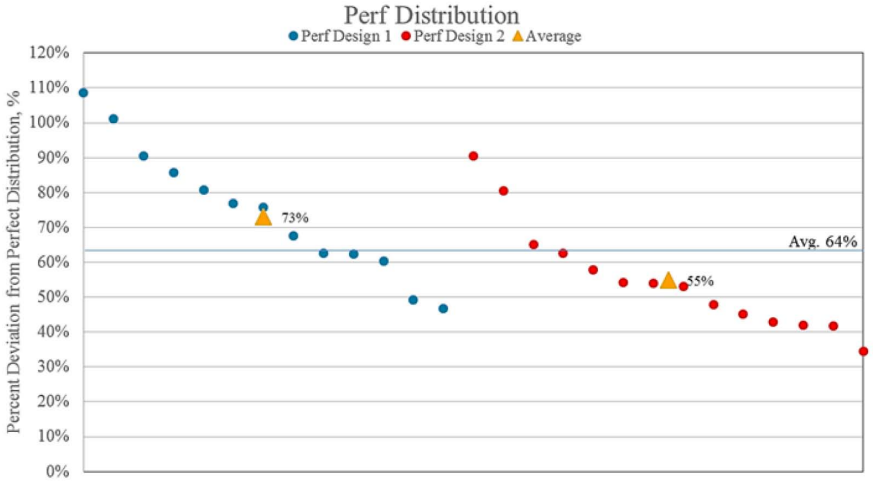

Figure 3— Percent deviation from perfect distribution of all clusters in a stage

Figure 4 shows the heelward bias of the total treatment on Well C. Nearly 50% of the designed treatment was placed in the two heel most clusters. On average, the heel cluster received more than twice as much treatment as the toe cluster.

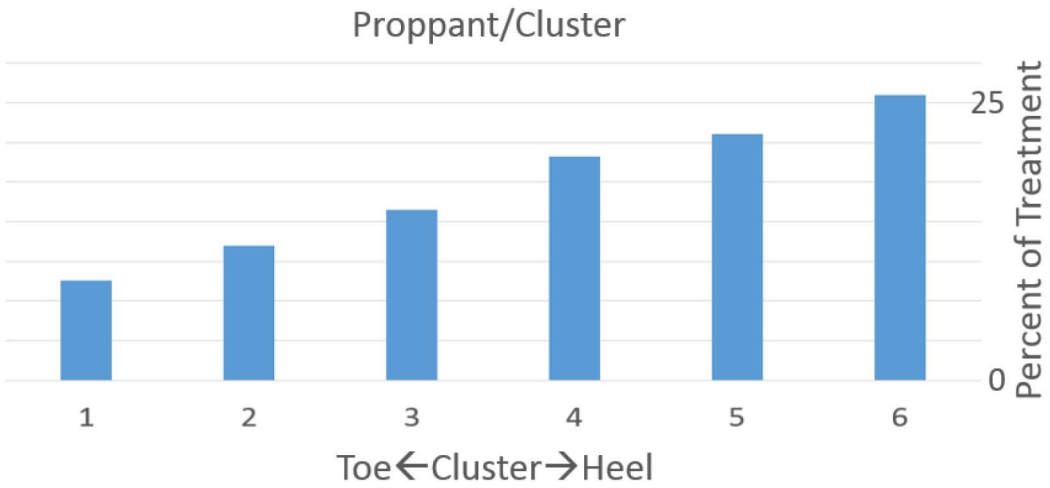

Figure 4— Average proppant distribution/cluster for total treatment of Well C

Along with the pre-planned variable testing, multiple optimizations of the pump design were discovered during the treatment of the fiber optic well (Well C) using the real-time DAS and DTS data. The pumping schedule was altered to test different ratios of slickwater and high viscous fluids, ratios of proppant sizes, and concentrations of proppant within the various fluids.

Figure 5 shows a trend recognized in multiple stages. A large pressure increase in surface treating pressure correlated to a quiet zone and warm back in the toe-side clusters of a treatment stage. After further analysis, when the larger proppant reached the perforations in a low viscous fluid, there was an inadvertent diversion away from the toe-side clusters towards the heel-side clusters. The pressure spike represented the sudden reduction of open entry holes in the wellbore, increasing perforation friction at the same pumping rate. The quiet zone confirms the lack of fluid and proppant entering the toe-side clusters, creating a lack of acoustic signal, the warm back further confirms the toe-side clusters not receiving fluid.

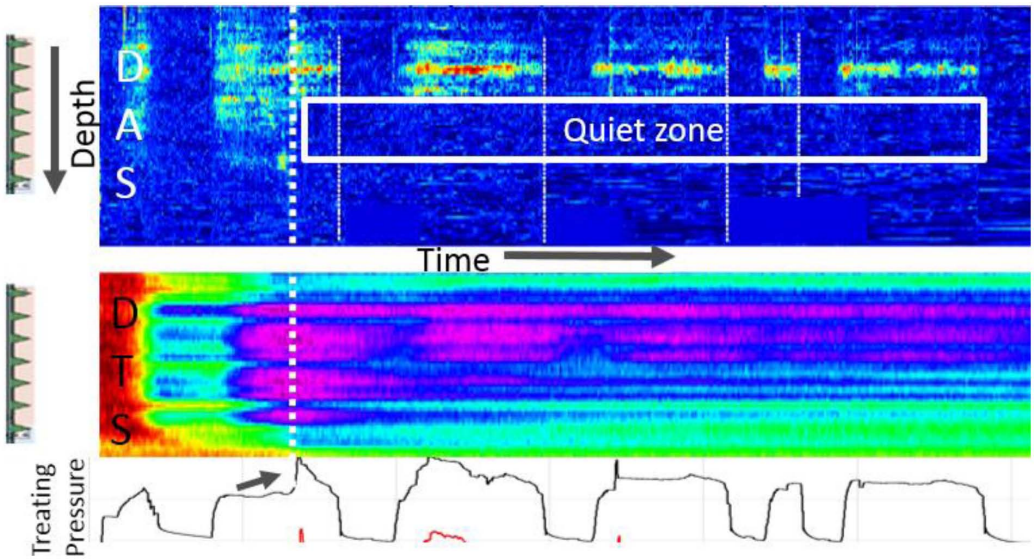

Figure 5— Fiber optic results, DAS and DTS, with treatment pressure, showing unintended diversion

By using the DAS and DTS to define the root of the problem, a shift in the pump schedule aligning proppants and fluid types mitigated the issue, leading to better cluster distribution in future stages and wells.

Borehole Microseismic

Borehole microseismic data was collected during the hydraulic fracture stimulation using five monitoring arrays. The five arrays consisted of one multipoint array, one horizontal array and two vertical arrays (Figures 6 and 7). Utilizing both vertical and horizontal arrays produced a high-quality data set with approximately 13,000 microseismic events recorded. 98% of the events were co-located over the 29 stages and over 8,000 events were recorded by all five arrays. The velocity model was calibrated throughout the stimulation with all 158 perforation locations being imaged and processed using a vertical seismic profile optimized velocity model. The error is calculated using a Monte Carlo algorithm to determine at what extent the velocity model breaks down. The median location error is 24 feet, the median depth component of error is 30 feet, which suggests more uncertainty in depth than in X, and Y.

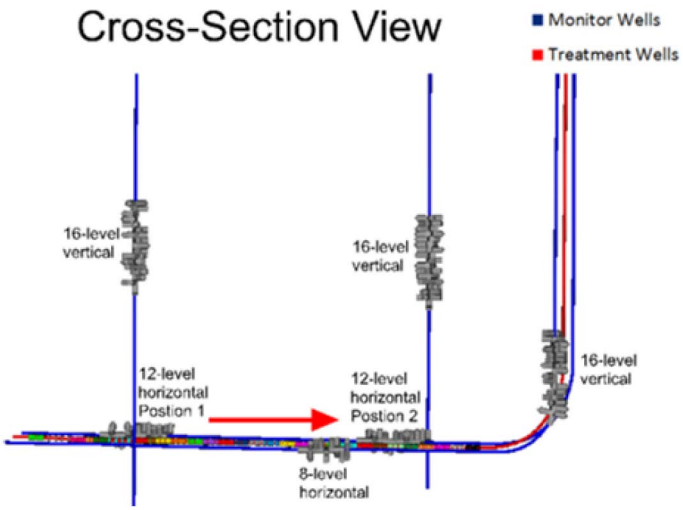

Figure 6— Array locations, cross-section view

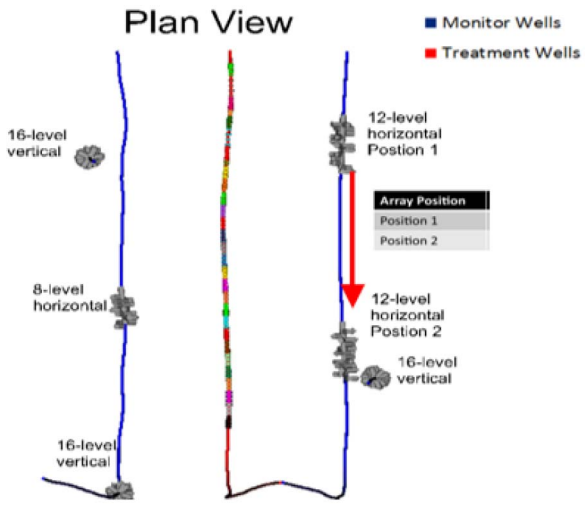

Figure 7— Array positions, plan view

The primary objectives of the microseismic project were to characterize the hydraulic fracture height and fracture length as well as optimize the treatment program. Completion parameters were modified along lateral and a detailed microseismic analysis of the various completion designs was performed.

Asymmetric fracture growth was identified along the lateral as well as changes in microseismic fracture geometry with varying completions types. Overall, the majority of the microseismic events were heavily concentrated in the treatment interval (Figure 8). Fracture azimuth remained consistent across all stages of the lateral. The heel-ward stages showed a greater height growth when compared to toe-ward and mid-lateral stages. Additionally, higher moment magnitude events were focused toward the heel.

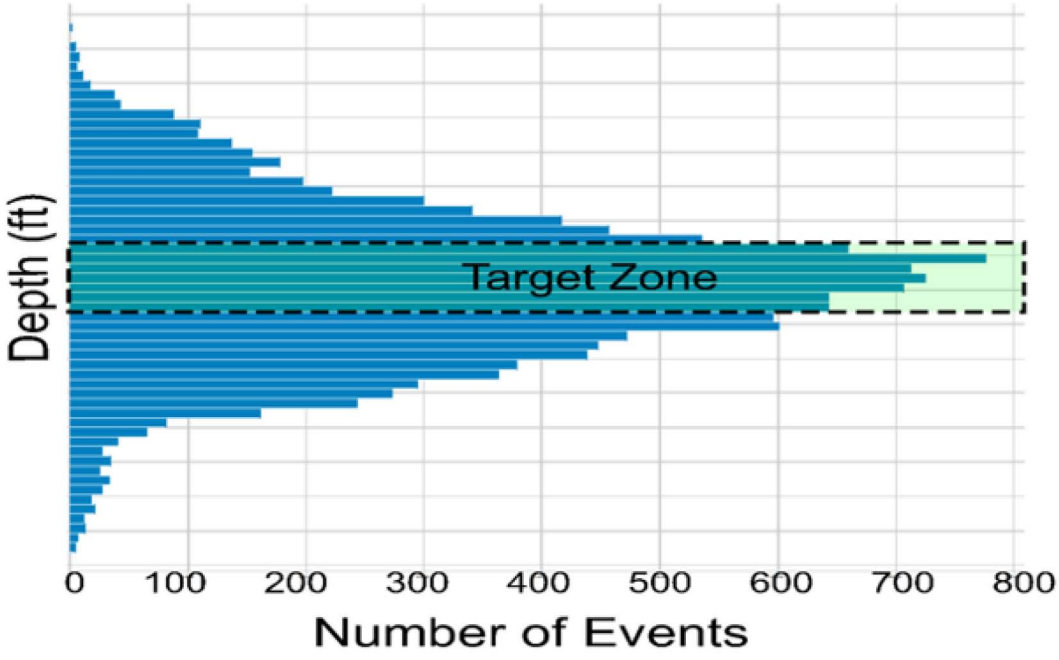

Figure 8— Depth vs Events, showing largest number of events in target interval

Electromagnetic Imaging

A novel, surface-based electromagnetic technique assisted in imaging the placement of hydraulic fracture fluids during completion operations of the test well. This technique used an electromagnetic transmitter situated above the well bore and an array of antennae to monitor fluctuations in the generated electromagnetic field. This novel technology is in contrast to other emerging electromagnetic tools, which require the transmitter to be stationed within the wellbore at depth.

Electromagnetic imaging depended upon a differencing approach to detect resistivity changes brought upon by introduction of completion fluids into the reservoir interval. An electromagnetic field was continuously generated by the surface transmitter. This field fluctuated in frequency according to a preset pattern, which allowed for the elimination of cultural electromagnetic "noise." The surface array took a record of the induced electromagnetic field every four seconds before, during, and after pumping began on each frac stage. Differences observed in the field were attributed to the introduction of water into the reservoir interval. Post-processing of the differences allow for spatial distribution of fracture fluids to be delineated (i.e. the fluid fracture half-length). At the current time, only a two-dimensional reconstruction of fluid emplacement is possible with this approach.

12 stages were successfully imaged electromagnetically. Fracture azimuths and half-lengths detected are well aligned with microseismic results (Figure 9). Resolution of the processed data was hindered by the decision to set up the surface antennae array out to 1000’ (E-W) away from the wellbore. A tighter and denser antennae array is recommended on future electromagnetic projects of this type. Other operational difficulties included errors in antennae and transmitter placement, high winds, and a lightning strike (which destroyed 30% of the antennae).

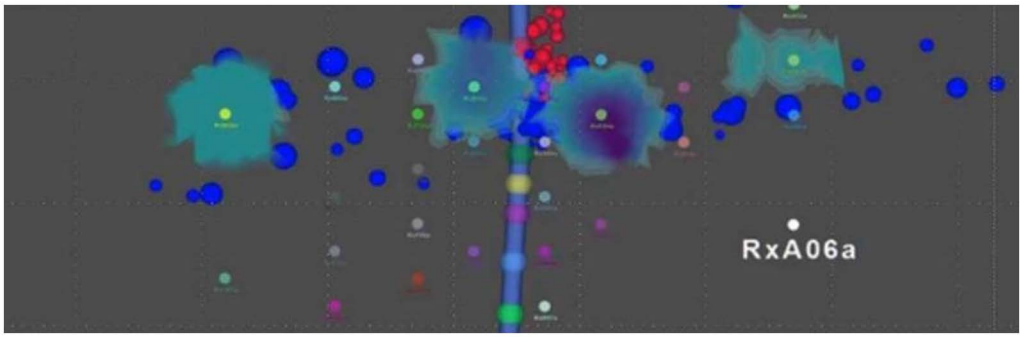

Figure 9— Electromagnetic Imaging (blue and aqua shapes) Showing Alignment with Microseismic (dots)

Offset Pressure Monitoring

High-resolution surface pressure transducers monitored the response of offset wells during stimulation. A technique that relates poromechanically induced signals in offset wells to fracture geometry was applied. The technique uses an Integrated Modeling Approach for Geometric Evaluation of Fractures, and is thus, referred to as IMAGE Frac (Dawson and Kampfer 2016). Results from the study provided hydraulic and propped heights, half-lengths, and fracture azimuth. The results corroborated well with the interference test, fiber data, and tracer data.

Figure 10 shows the raw pressure signal from an isolated stage in the heel of Well C while stimulating adjacent wells A, B, and D). Each colored interval on the timeline corresponds to the stimulation of a stage. When the toe stages of the wells being stimulated are completed, the poroelastic pressure signals are small, but as the stages toward the heel are completed (in closer proximity to the observation stage in C), the poroelastic signals get larger.

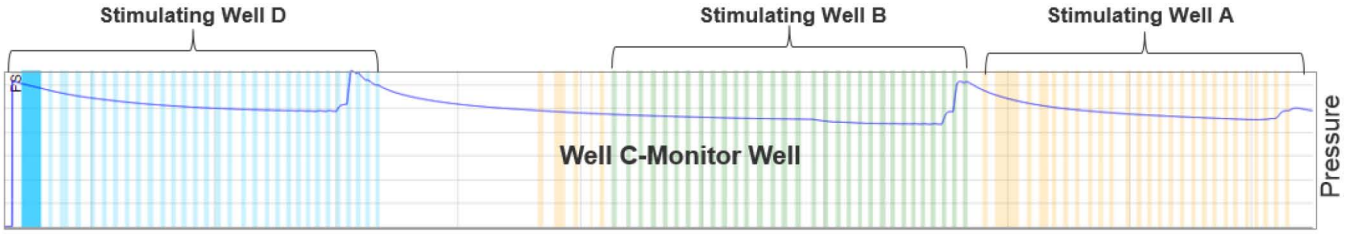

Figure 10— Offset pressure monitoring

Figure 11 plots the magnitude of the poroelastic signal observed in an observation stage versus the stage number of an adjacent well being stimulated. In Figure 11, the observation stage is closest in proximity to stage 5 of the stimulated well, and the peak poroelastic response is observed when completing stage 5.

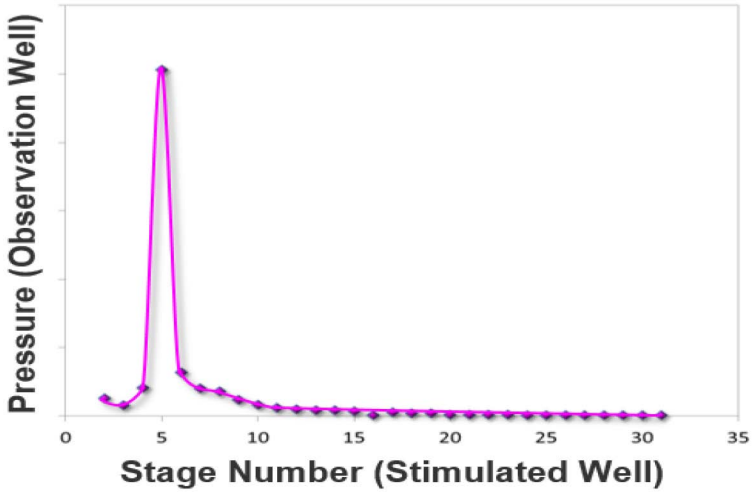

Figure 11— Offset pressure monitoring

Using the poroelastic pressure signals, the IMAGE Frac approach was used to evaluate the geometry of the largest fracture in each stage. Figure 12 shows a gun barrel view of the average geometry of the largest fracture in each stage.

Figure 12— Gun barrel view of the average geometry of the largest fracture in each stage.

A measure of the uncertainty can be determined by comparing the fracture half-lengths in a single well as determined from two different monitor locations. Table 1 shows the normalized fracture half-length of the largest fracture in several stages in Well D as measured from two different observation wells (Well C & Well E). The variation in measurements of the fracture half-lengths of Well D from Well C and Well E ranges from 1-14% with a mean of 7%.

Table 1— Normalized fracture half-lengths of the largest fracture in each stage of Well D as measured from Well C & Well E.

Well D	Fracture Half Length		
Stage	E Gauge	C Gauge	% Diff
22	1.18	1.13	4%
23	1.14	1.20	5%
24	1.04	0.99	5%
25	0.98	0.93	5%
26	0.88	0.81	7%
27	1.04	1.03	1%
28	1.08	1.25	14%
29	0.90	0.81	10%
30	0.91	0.98	6%
31	0.88	0.96	9%
AVERAGE	**1.00**	**1.01**	**7%**

The IMAGE Frac technology was also used to evaluate the effectiveness of diverter at improving the fluid distribution across the stage. The impact of several hundred diverter drops of various sizes was examined. Figure 13 shows the impact of diverter drop size on the fluid distribution across the stage. In a majority of the drops, the fluid distribution was not deemed to have been significantly impacted; however, for all drop

sizes examined, over 30% of the time the diverter improved fluid distribution. Moreover, in more than 10% of the drops, diverter significantly improved fluid distribution.

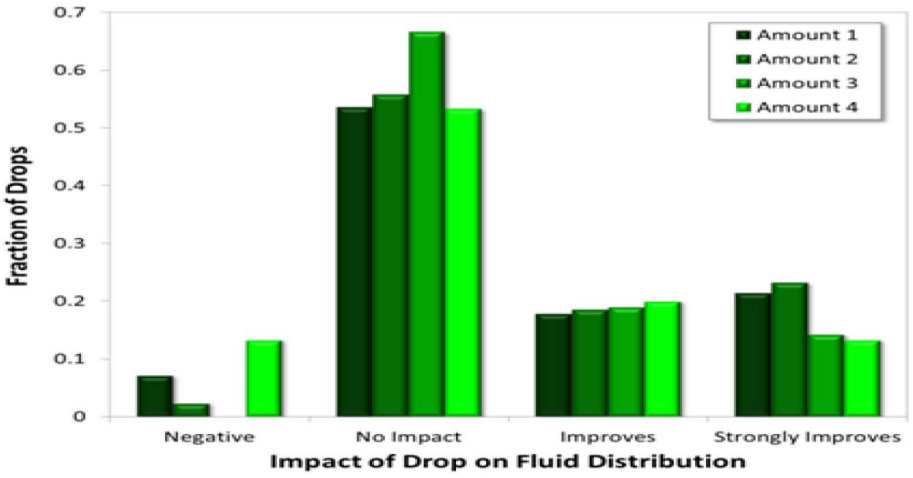

Figure 13— Impact of diverter drop size on fluid distribution along the lateral.

Figure 14 shows the impact highly effective diverter drops can have on the fluid distribution along the stage. The ratio of the 2nd largest fracture to the 1st largest fracture is plotted for three different completions designs. The larger the ratio, the better the fluid distribution along the lateral. In the base case, the median ratio is close to 0.45. In the case of highly effective diverter, the median ratio increases to close to 0.75, a significant improvement in fluid distribution. Figure 14 also shows a new completion design, which improved the fluid distribution even further.

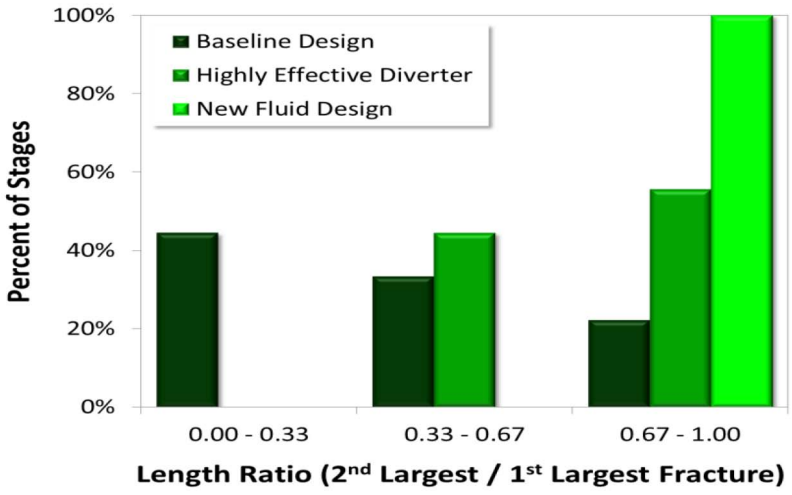

Figure 14— Comparison of ratio of the 2nd largest fracture length to the 1st largest fracture length for three different completions designs.

Diverter Analysis

Fiber optic monitoring was used to evaluate diverter effectiveness. Figure 15 is an example of successful diversion. The DAS plot (top) shows a shift in the location of the acoustic response after diverter was injected at point B and again at point C. The signature is validated through the cool down of the same clusters that showed increased acoustic response at points B and C.

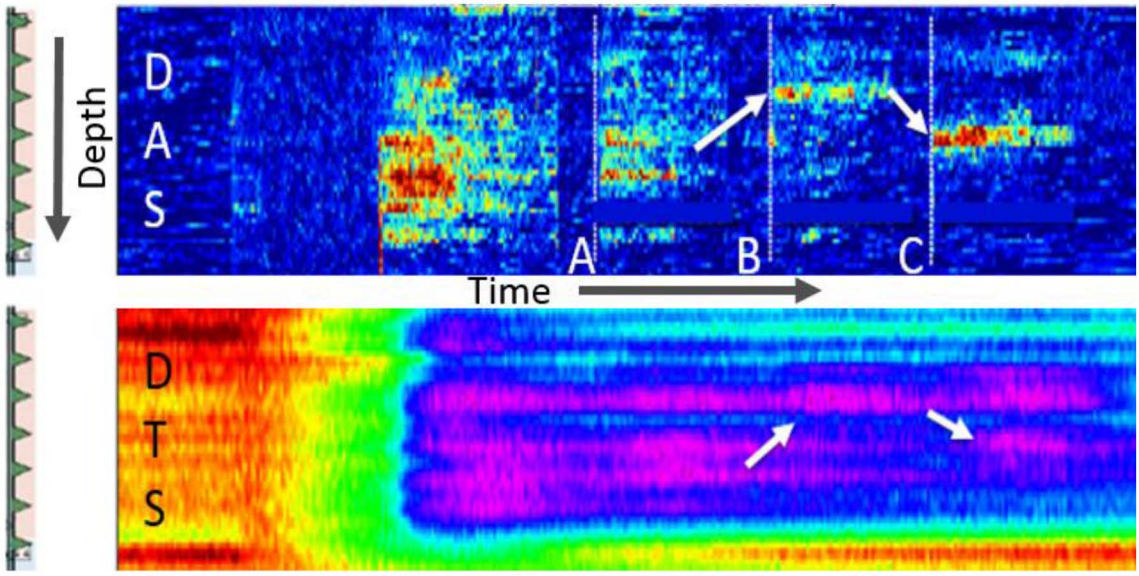

Figure 15— DAS and DTS showing successful diversion

Average cluster efficiency ranged from 33%-75% during the treatment of the fiber optic well. Changes ranging from fluid type to proppant size appeared to be the source of acoustic signal changes. A series of diversion tests were performed in attempt to improve cluster efficiency. Figure 16 compares the four techniques and the range of results. Diverter B showed the highest rate of success in stopping fracture growth. Diverter C showed no ability to stop fracture growth but never caused accelerated growth. Diverters A and B most commonly showed no impact or an acceleration of the dominant fracture.

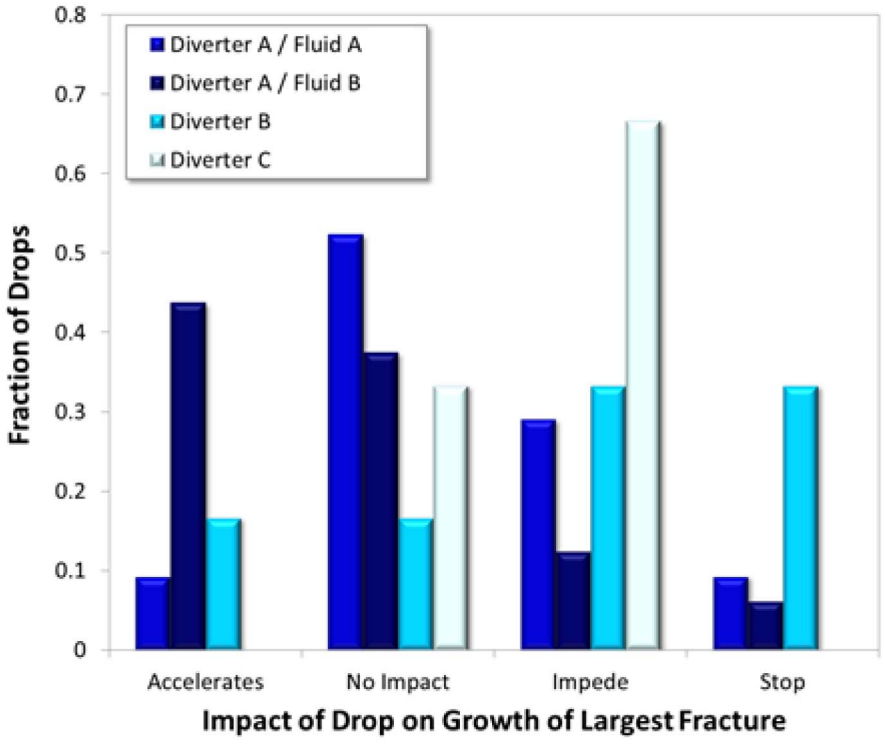

Figure 16— Varying diverter and fluid comparison

Water Hammer Analysis

The water hammer model proposed by Mondal (2010), Carey (2014), and Carey et al. (2015) was used to history-match the water hammer signal at multiple rate drops and at the conclusion of pumping the stage. The purpose of the analysis was to correlate water hammer responses to fracture geometry. Hydraulic half-lengths from the analysis are similar to the microseismic geometry. High frequency pressure data was collected during stage treatment to provide improved resolution for the matching process. The model combines the hydrodynamic equations of the wellbore, derived from the conservations of mass and momentum, with a fracture modeled by simple series circuit with resistance (R), capacitance (C), and inertance (I) (Carey et al, 2016). Figure 17 is a plot of treating pressure with four separate water hammer events, Figure 18 is an example of a matched water hammer event.

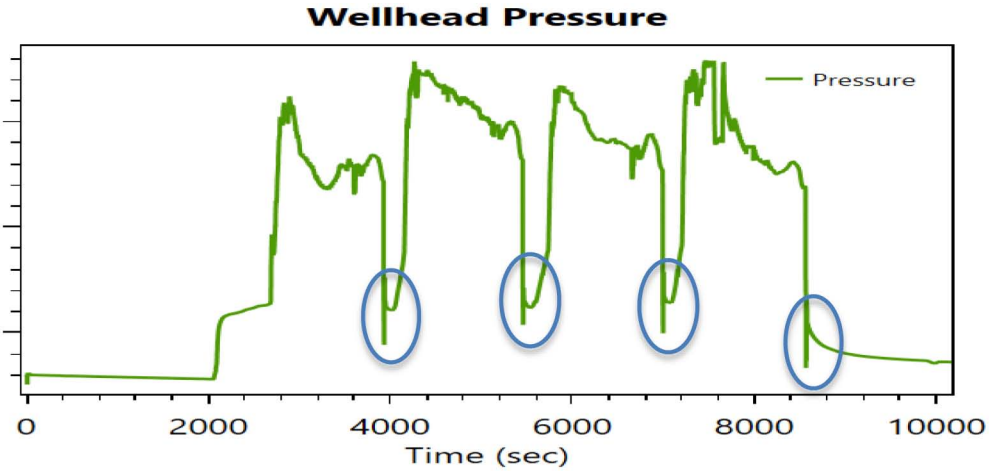

Figure 17— Events Modeled

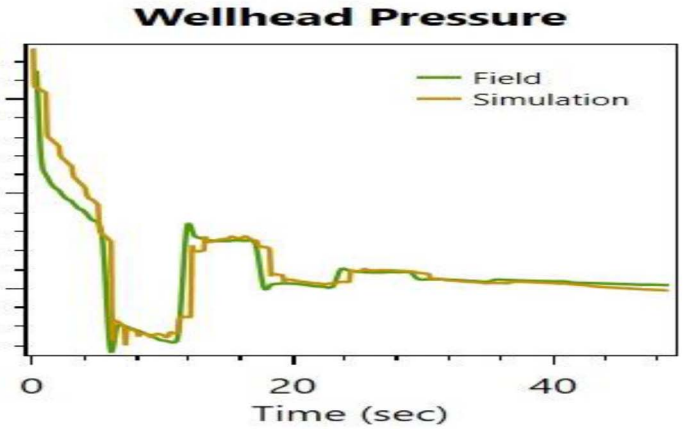

Figure 18— Matched Water Hammer Event-Jongsoo Hwang

Fracture Modeling

A planar 3D finite difference fracture model was utilized for the simulation process. Vertical openhole logs from an offset well were imported to construct the stress profile and populate the reservoir properties. A Diagnostic Fracture Injection Test (DFIT) was performed in a horizontal well offsetting the fiber optic well, the DFIT provided fracture gradient, closure gradient, and pore pressure gradient. History matching of multiple stages from the horizontal completion provided confidence in the modeled parameters. Figure 19 is the stress grid for the model, the lateral placement is shown at the base of a lower stress interval.

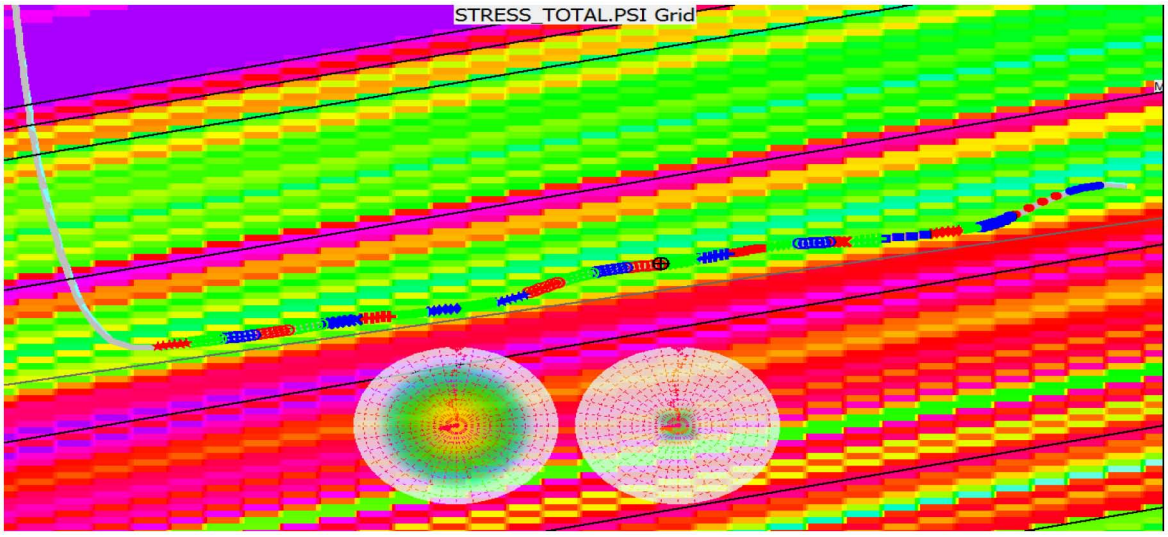

Figure 19— Stress profile

A calibrated vertical model using the properties derived from the openhole logs, DFIT, and history matching of the horizontal completion was used to run sensitivities on fracture geometry based upon actual proppant placed. Figure 20 shows the conductive geometry variations as a function of proppant placed in the fracture, 100% represents even proppant distribution in all fractures. The purpose of modeling various volumes of proppant placed in a fracture was to allow for a more accurate description of the fracture geometry based on the results from the fiber optic analysis.

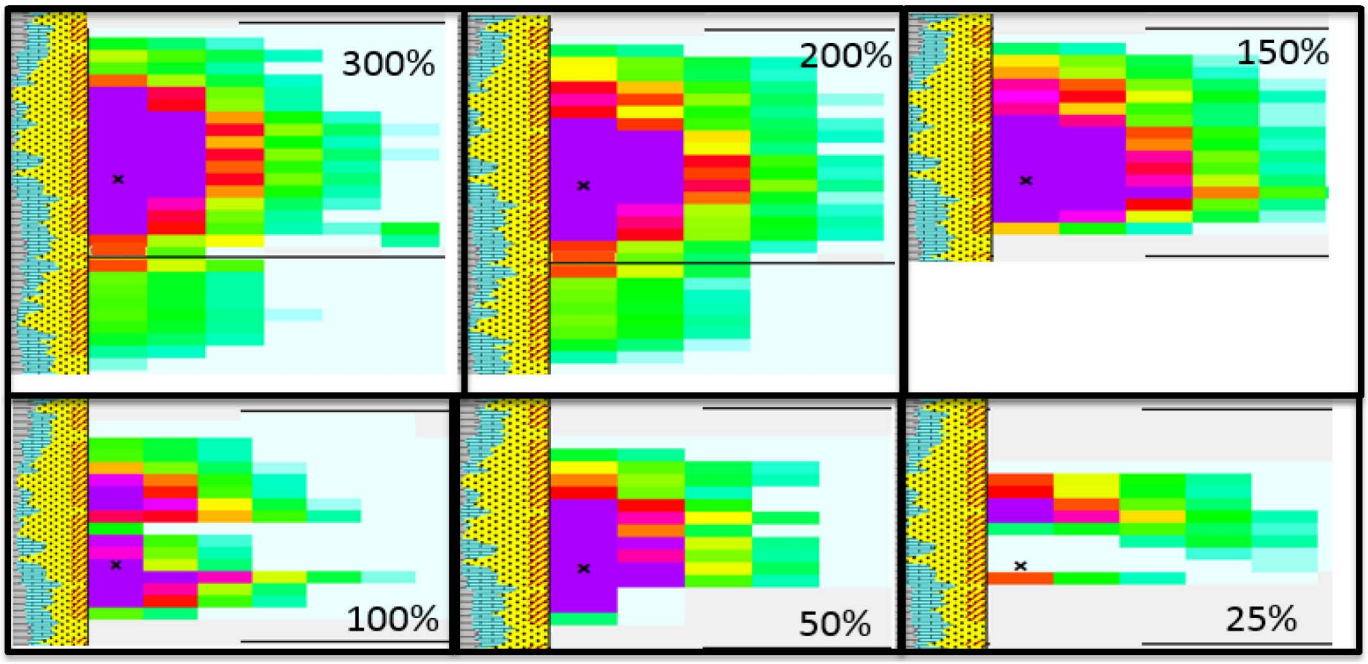

Figure 20— Conductive geometries for range of proppant placed relative to design

Validation Tools

The fiber optic well (Well C) included a borehole pressure gauge allowing for a high quality interference test. Post completion of the Well C and both offsets (Well B and Well D), an interference test was performed. Pressure and gas rates were monitored to quantify the amount of interaction between the wells at the current

spacing. The plot below depicts the bounding wells' (Well B and Well D) gas rates in red and green and the bounded well (Well C) in black. Well B and Well D were shut in for a period of time, there was no increase in production for the bounded well (WellC). The results from the interference test shown in Figure 21 suggest that the wells are not in communication with one another.

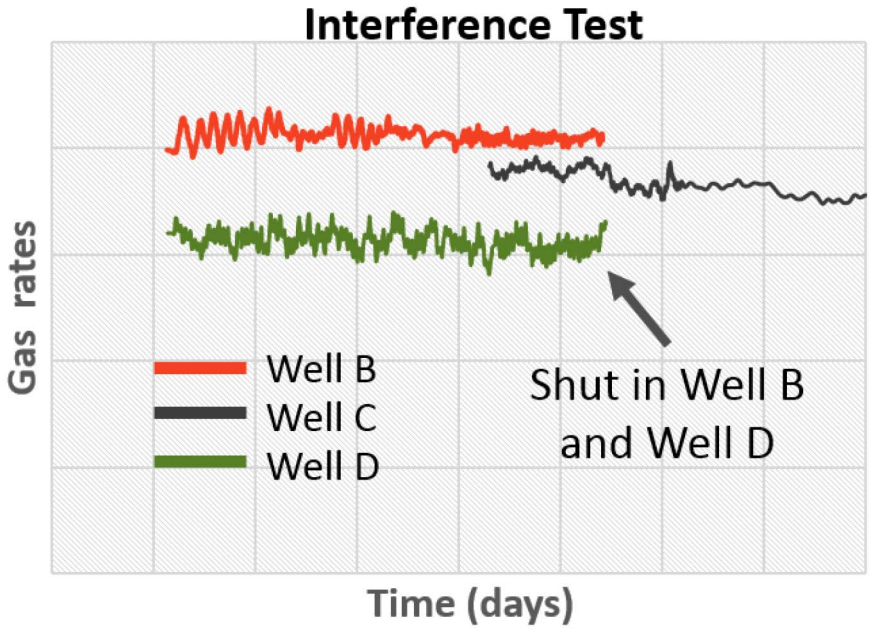

Figure 21— Interference test, gas production

There was no effective production impact and minimal pressure communication. Given the lack of observed well-to-well communication, it was determined that effective fracture half-lengths do not overlap between the bounding wells (Well B and Well D) and the middle well (Well C). The lack of interference between the wells led to increased well density in future spacing pilots.

Oil Soluble Tracer (OST) and Fracture Fluid Identifier (FFI) introduced to the formation during stimulation provided insight to propped and hydraulic geometries. In order to qualify geometries from the use of tracers, symmetric half-lengths were assumed. FFI was recovered in the well offsetting the treatment well; OST was not recovered in offsetting well. Based upon a symmetric fracture assumption, the hydraulic half-length exceeds 0.5X lateral well spacing, and propped half-length is less than 0.5X lateral well spacing.

Rate Transient Analysis (RTA) was performed on Well C after three months of production to quantify fracture geometry ranges. The fiber optic results improved the RTA by providing an accurate description of the number of treated fractures. Results from the interference test were integrated into the RTA to provide half-length constraints. The resulting height from RTA after applying the constraints outlined above agreed with the fracture model and offset pressure monitoring.

Conclusions

A multi-disciplined team utilized their methods and results to optimize field development and future spacing pilots. Table 2 compares the normalized geometries measured by the various technologies; each column is normalized to the average dimmension. Offset pressure monitoring, RTA, and fracture modeling corroborated well in the description of conductive fracture height. Microseismic, electromagnetic imaging and offset pressure monitoring provided azimuths within ten degrees of one another. The agreement between multiple diagnostic tools increased our confidence in the fracture geometry. Integration of the diagnostic tools has led to an improved understanding of hydraulic, propped, and conductive fracture geometries and optimal well spacing.

Table 2—Summary of geometries

Diagnostic Tool	Hydraulic		Propped		Conductive		Azimuth
	Xf	Hf	Xf	Hf	Xf	Hf	degrees
EM Imaging	0.6u	-	0.9w	-	-	-	10+A
Microseismic	1.3u	1.5v	-	-	-	-	0+A
Offset Pressure	0.8u	0.7v	1.1w	0.9x	-	-	1+A
Frac Model	1.2u	0.8v	1.4w	1.1x	0.9y	1z	-
Tracer	>0.5u	>0.7v	>0.75w	>0.5x	<3y	>0.5z	-
Interference Test	-	-	<0.9w	-	<3y	>0.5z	-
Analytical Model	-	-	-	-	0.9y	1z	-
Water Hammer	1.5u	0.8v	-	-	-	-	-

Acknowledgments

The authors want to acknowledge Devon Energy for supporting the project and for permission to publish this paper. We also recognize Devon's Strategic Innovation Team for recommending and funding two of the technologies applied, and the execution teams involved with the installation of the plethora of diagnostic monitoring equipment. We would also like to recognize the service providers that contributed to making this project successful, and the work Jongsoo Hwang, University of Texas, provided through water hammer analysis.

References

Ugueto, G. A., Ehiwario, M., Grae, A., Molenaar, M., Mccoy, K., Huckabee, P., & Barree, B. (2014, February 4). Application of Integrated Advanced Diagnostics and Modeling To Improve Hydraulic Fracture Stimulation Analysis and Optimization. *Society of Petroleum Engineers*. Doi: 10.2118/168603-MS

Mondal, S. 2010. *Pressure Transients in Wellbores: Water Hammer Effects and Implications for Fracture Diagnostics*. M.S. Thesis. The University of Texas at Austin. Austin, TX

Carey, M.A. 2014. *Water Hammer Fracture Diagnostics*. M.S. Thesis. The University of Texas at Austin, Austin, TX

Carey, M.A., Mondal, S., Sharma, M.M. 2015. Analysis of Water Hammer Signatures for Fracture Diagnostics, Paper SPE 174866 presented at the 2015 SPE Annual Technical Conference and Exhibition, Houston, TX, 28-30 September.

Carey, M.A., Mondal, S., Sharma, M.M., Hebert, D.B., 2016. Correlating Water Hammer Signatures with Production Log and Microseismic Data in Fractured Horizontal Wells. Paper SPE 179108 presented at the 2015 SPE Hydraulic Fracturing Technical Conference, The Woodlands, TX, 9-11 February.

Dawson, M., Kampfer, G., 2016. Breakthrough in Hydraulic Fracture & Proppant Mapping: Achieving Increased Precision with Lower Cost, Paper SPE 2432330 presented at the 2016 Unconventional Resources Technology Conference (URTeC), San Antonio, TX, 1-3 August. DOI 10.15530/urtec-2016-2432330

Wheaton, B., Haustveit, K., Deeg, W., Miskimins, J., Barree, R., 2016. A Case Study of Completion Effectiveness in the Eagle Ford Shale Using DAS/DTS Observations and Hydraulic Fracture Modeling. Paper SPE 179149 presented at the 2015 SPE Hydraulic Fracturing Technical Conference, The Woodlands, TX, 9-11 February.